JGR Earth Surface

RESEARCH ARTICLE
10.1029/2021JF006218

The Influence of Sediment Transport on Stationary and Mobile Knickpoints in River Profiles

Stefan Hergarten[1]

[1]Albert-Ludwigs-Universität Freiburg, Institut für Geo- und Umweltnaturwissenschaften, Freiburg, Germany

Key Points:

- The simple stream power incision model extended by sediment transport does not predict knickpoint smearing in river profiles
- Neglecting sediment transport in analyzing a given river profile underestimates the velocity of knickpoint migration
- Stationary tectonic knickpoints are not immediately steady if sediment transport is taken into account

Correspondence to:

S. Hergarten,
stefan.hergarten@geologie.uni-freiburg.de

Citation:

Hergarten, S. (2021). The influence of sediment transport on stationary and mobile knickpoints in river profiles. *Journal of Geophysical Research: Earth Surface*, *126*, e2021JF006218. https://doi.org/10.1029/2021JF006218

Received 15 APR 2021
Accepted 3 NOV 2021

Abstract The analysis of stationary and mobile knickpoints has been one of the most powerful concepts in tectonic geomorphology for decades. While several models combining bedrock incision and sediment transport are available, the existing theory of knickpoints focuses on detachment-limited erosion without consideration of sediment transport. On the other hand, fully transport-limited systems do not maintain distinct knickpoints. This study addresses the existence and the properties of slope-break knickpoints in fluvial systems between the two extremes with the help of the shared stream-power model, which allows for a continuous shift between detachment-limited and transport-limited erosion. The most important result is that both stationary and mobile knickpoints remain sharp and are not smeared by sediment transport. The system responds to tectonic signals in two phases where the first phase is similar to the detachment-limited model. Comparing rivers with the same equilibrium profile at a given uplift rate, the velocity of knickpoint migration increases toward transport-limited conditions. The second phase of the response is dominated by changes in sediment flux and affects the entire river segment downstream of the mobile knickpoint including the fault where the tectonic signal was initiated. During this phase, the mobile knickpoint is flattened in the sense that the difference in steepness index across a slope-break knickpoint decreases through time. It is also shown that large parts of the theory for the nonlinear model, in particular knickpoint sharpening and stretching, remain valid, but the effect of nonlinearity decreases with increasing contribution of sediment transport.

Plain Language Summary Knickpoints are either breaks in slope along a river or even almost vertical steps, or waterfalls. While knickpoints can be generated by a variety of phenomena, sudden changes in tectonics or climate typically generate knickpoints that are moving upstream over geological time scales. If preserved, such mobile knickpoints provide an archive of the tectonic or climatic history. The existing theory of knickpoints is based on a simple erosion model where the effect of sediment transport is neglected. This study extends the theory by the effect of sediment transport. As a main result, the occurrence of knickpoints is not affected by sediment transport, but their properties change. So we cannot conclude from the occurrence of mobile knickpoints that the effect of sediment transport on the evolution of the respective river segment is negligible. When analyzing a given river segment quantitatively, neglecting sediment transport can result in misinterpretations. In particular, the velocity of knickpoint migration will be underestimated. This also implies that a given river segment carries information over a shorter time span than usually assumed.

1. Introduction

Knickpoints are typically defined as abrupt changes in channel slope along a river profile. While conceptual work on knickpoints dates back to the 19th century (Davis, 1899), knickpoints are nowadays widely used for deciphering the tectonic history. The basic types of knickpoints, their generation, and their fundamental properties can be illustrated by the three scenarios sketched in Figure 1, where the fundamental concept is that erosion rates increase with increasing channel slope and that erosional signals propagate upstream through time.

Initiating an ongoing vertical displacement at a fault (Figure 1a) results in a discontinuity in uplift rate along the river. As a consequence, a steeper river segment emerges above the fault and expands upstream through time. While the channel slope of this segment is already adjusted to the increased uplift rate, the rest of the river profile still reflects the original conditions. The channel slope changes abruptly at the edges of this river segment, resulting in a pair of knickpoints. The upper knickpoint moves upstream, whereas the lower knickpoint stays at the fault.

While this scenario describes slope-break knickpoints, a sudden vertical offset (e.g., by a strong earthquake) may result in a second type of knickpoint (Figure 1b), typically called topographic-step knickpoint (e.g., Whipple

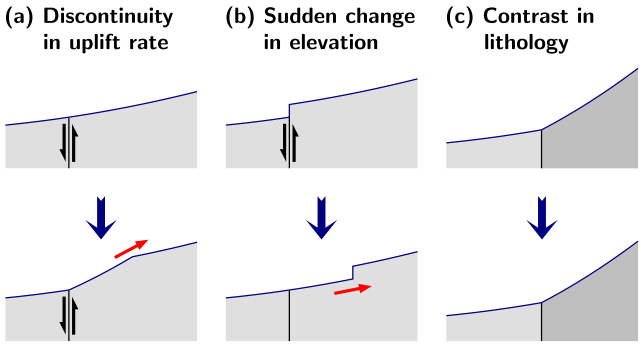

Figure 1. Three scenarios of knickpoint formation and migration.

et al., 2013). Since the erosion rate is high in the steep segment, it migrates upstream, but does not necessarily leave a persistent signature at the fault itself. Topographic-step knickpoints are typically visible as a waterfall and are thus recognized more easily in field than slope-break knickpoints. Conceptually, however, slope-break knickpoints can be seen as the more fundamental type of knickpoint since a topographic-step knickpoint can be equally described as a steep reach bound by slope-break knickpoints on either side.

Owing to the apparently simple behavior of mobile knickpoints at least on a qualitative level, they can often be seen as a window into the tectonic history. However, the occurrence of knickpoints is not necessarily related to active tectonics or other time-dependent conditions. As illustrated in Figure 1c, a contrast in lithology with a vertical interface may result in a knickpoint which is not only stationary at the interface, but also may even be completely steady. If the interface is not vertical, lithologic knickpoints will also migrate. There are several further scenarios where knickpoints may occur, for example, vertical-step knickpoints as the result of a caprock with a high resistance against erosion (Haviv et al., 2010). Beyond this, the effect of climatic signals on river profiles may be similar to those of tectonic signals. However, discussing these scenarios in detail would go beyond the scope of this study.

Investigating knickpoints in the context of the tectonic history is attractive since it can be done on a qualitative level without the need for running numerical simulations. While the occurrence of knickpoints can be interpreted qualitatively using simple concepts such as those illustrated in Figure 1, several computer-based tools for assisting the manual delineation or for the automatic detection of knickpoints have become available (e.g., Gailleton et al., 2019; Neely et al., 2017; Queiroz et al., 2015; Schwanghart & Scherler, 2014).

Mobile knickpoints are typically considered in the context of detachment-limited erosion (Howard, 1994). The idea behind this concept is that all particles entrained by the river are immediately swept out of the system. The stream-power incision model (SPIM) is widely used in this context and is the key component of several models of large-scale fluvial landform evolution (for an overview, see, e.g., Willgoose, 2005; Wobus et al., 2006). It predicts the erosion rate E as a function of the upstream catchment size A and the channel slope S in the form

$$E = KA^m S^n. \tag{1}$$

If the exponents m and n were universal properties of the erosion process, the parameter K would be the only model parameter. The parameter K is typically called erodibility. While this term suggests that it is primarily a property of the river bed, it is in fact a highly lumped parameter that subsumes all dependencies of E except for A and S, for example, precipitation.

The problem with the exponents m and n is that only their ratio is well-constrained by real-world data. In his seminal study of longitudinal river profiles, Hack (1957) proposed the relation

$$S \sim A^{-\theta}, \tag{2}$$

where θ is nowadays called concavity index. According to Equation 1, a river segment with constant K at a spatially uniform erosion rate E satisfies this relation if $\frac{m}{n} = \theta$. While Hack (1957) obtained $\theta > 0.5$ in the mean, contemporary studies use either $\theta = 0.45$ or $\theta = 0.5$ as a reference value (e.g., Lague, 2014; Whipple et al., 2013).

The absolute values of the exponents m and n are more uncertain than their ratio since they cannot be determined from the shape of equilibrium profiles under uniform erosion. Assuming $n = 1$ simplifies both theoretical considerations and the numerical implementation since the model is linear with regard to S and thus also with regard to to the surface elevation H then. In turn, the results compiled by Lague (2014) as well as some recent studies (Adams et al., 2020; Harel et al., 2016; Hilley et al., 2019) rather suggest $n > 1$.

Inserting the SPIM into the equation of landform evolution,

$$\frac{\partial H}{\partial t} = U - E, \tag{3}$$

where U is the rate of uplift of crustal material relative to a given datum, yields a hyperbolic differential equation of the advection type. Propagation of information in one direction only—upstream here—is a characteristic property of this type of differential equation. Anything that happens at a given point and a given time only affects the region upstream of this point in the future. So the SPIM is the simplest landform evolution model that captures the concepts described in Figure 1.

The analysis of longitudinal river profiles in the context of the SPIM was simplified by the χ transform introduced by Perron and Royden (2013). It transforms the along-stream coordinate x to a new coordinate

$$\chi = \int \left(\frac{A(x)}{A_0} \right)^{-\theta} dx, \tag{4}$$

where A_0 is an arbitrary reference catchment size and the integration is performed along the river in upstream direction, starting from an arbitrary reference point. While A_0 was introduced in order to avoid inconvenient physical units of χ for $\theta \neq 0.5$, the equations are simpler without A_0. So let us omit A_0 in the following. Then, Equation 4 yields

$$\frac{d\chi}{dx} = A^{-\theta}. \tag{5}$$

While the original channel slope is $S = \frac{\partial H}{\partial x}$ (where x increases upstream), the slope of the χ-transformed profile is

$$\frac{\partial H}{\partial \chi} = \frac{\frac{\partial H}{\partial x}}{\frac{d\chi}{dx}} = A^{\theta} S. \tag{6}$$

This property is also known as the steepness index k_s. The SPIM can then be written in the form

$$E = K \left(\frac{\partial H}{\partial \chi} \right)^{n}. \tag{7}$$

Thus, χ-transformed river profiles with constant K at a uniform erosion rate are straight lines, where tributaries are collinear to the trunk stream.

A theory for the migration of knickpoints based on the χ transform was developed by Royden and Perron (2013). It was found that knickpoints migrate upstream at a constant velocity along the χ-axis for $n = 1$. While Royden and Perron (2013) used a nondimensionalization where the velocity is unity, the velocity is K in the formulation used here. This result can be obtained by inserting Equation 7 into Equation 3, but will also be recovered in Section 6. In turn, the velocity along the original coordinate x is KA^{θ} (e.g., Beckers et al., 2015) and thus not constant. For $n \neq 1$, however, the behavior is more complicated. The respective theory developed by Royden and Perron (2013) will be extended in Section 10.

However, sediment transport has an effect on erosion even in bedrock channels (e.g., Turowski, 2012), which questions the simple idea behind the SPIM that all entrained particles are immediately swept out of the system without any further effect. Any extension of the SPIM where the sediment flux affects the erosion rate changes the mathematical properties of the model fundamentally. While information propagates only upstream in the SPIM, the downstream flux of sediments introduces a downstream propagation of information. So signals typically propagate in both directions in mixed incision-transport models.

Whipple and Tucker (2002) formulated a simple extension of the SPIM toward sediment transport in the form

$$E = K \left(1 - \frac{Q}{Q_c} \right) A^m S^n, \tag{8}$$

where Q is the actual sediment flux (volume per time) and Q_c the transport capacity. Since the erosion rate decreases linearly with increasing sediment flux, this model is called linear decline model. The transport capacity Q_c defines the sediment flux at which net erosion turns into a net deposition of sediment.

Whipple and Tucker (2002) also proposed a generic formulation of the tools-and-cover concept based on ideas of Sklar and Dietrich (1998). The idea behind this concept even dates back to Gilbert (1877). In contrast to the linear decline model, the tools-and-cover concept assumes that a moderate sediment flux increases the rate of incision by enhancing abrasion and creating fractures, while a large sediment flux shields the bed and thus reduces erosion. Whipple and Tucker (2002) implemented this concept by replacing the linear dependency on $\frac{Q}{Q_c}$ in Equation 8 by a parabolic term. The linear decline model was interpreted as a reduction of the tools-and-cover concept to the cover effect in subsequent studies (Gasparini et al., 2006, 2007), where the ratio $\frac{Q}{Q_c}$ is considered as the degree of alluvial cover.

While the linear decline model is a generic model, the ξ-q model

$$E = KA^m S^n - G\frac{Q}{A} \tag{9}$$

proposed by Davy and Lague (2009) starts from a simple approach for the settling velocity of particles. The symbol G follows the notation of Yuan et al. (2019) since the symbol Θ used by Davy and Lague (2009) might be confused with the concavity index θ. The nondimensional parameter G involves the settling velocity and the vertical distribution of the particles and the precipitation rate. On a more generic level, it controls the transition from the SPIM ($G = 0$) toward the transport-limited regime. It is easily recognized by comparing Equations 8 and 9 that the ξ-q model can be seen as a specific version of the linear decline model with

$$Q_c = \frac{K}{G}A^{m+1}S^n. \tag{10}$$

As a main property of the ξ-q model, rivers at a spatially uniform erosion rate satisfy Hack's relation (Equation 2) with the same θ for all values of G. As pointed out by Whipple and Tucker (2002), the rivers studied by Hack (1957) already covered a wide range from detachment-limited to transport-limited conditions without a systematic difference in the concavity index θ. In the context of the linear decline model, this finding suggests that the transport capacity must be proportional to $A^{m+1}S^n$ (Equation 10), and the ξ-q model provides some justification of this approach from a simplified model of settling particles.

However, Equation 10 reveals that the ξ-q model may be more complex than it seems at first. The definition of G based on a settling velocity includes no obvious dependence on the properties of the bedrock. So a low erodibility of the channel bed would result in a low transport capacity. In reality, however, settling particles would rapidly built up an alluvial cover with an erodibility K much higher than that of the bedrock. The SPACE model (Shobe et al., 2017) implements this concept by relating the thickness of the cover to the roughness of the bed.

Efficient numerical implementations of the ξ-q model using a fully implicit time step have recently become available, which make the model more attractive for large-scale simulations over long time spans. While the scheme presented by Yuan et al. (2019) involves a fixed-point iteration for the sediment flux that converges rapidly as long as G is not too large, Hergarten (2020b) proposed an even more efficient direct solver without this limitation for the linear model ($n = 1$).

2. The Shared Stream-Power Model

While the ξ-q model directly refers to incision and sediment deposition, the mathematically equivalent formulation

$$\frac{E}{K_d} + \frac{Q}{K_t A} = A^m S^n = \left(\frac{\partial H}{\partial \chi}\right)^n \tag{11}$$

proposed by Hergarten (2020b) returns to a generic level. This model contains two erodibilities, where K_d describes the erodibility in absence of transported sediment and is the same as K in the linear decline model and in the ξ-q model. In turn, K_t characterizes the ability to transport sediment at zero erosion. Since this formulation describes a sharing of the stream-power term $A^m S^n$ between incision and sediment transport, the term "shared stream-power model" was suggested. The shared stream-power model turns into the original SPIM for $K_t \to \infty$ and into a transport-limited model for $K_d \to \infty$.

The shared stream-power model is a specific version of the linear decline model with $K = K_d$ and $Q_c = K_t A^{m+1} S^n$. So it contains no tools effect in the sense of the tools-and-cover concept. An interpretation as the cover component would be possible, but would be an unnecessary narrowing of the generic concept of sharing stream power between incision and sediment transport.

At this point, it should be emphasized that the erodibility K_d refers to the actual river bed, which may differ strongly from the erodibility of the bedrock if a thick alluvial cover is eroded. The erodibility of a fresh alluvial cover is typically much higher than that of the bedrock, so that the model would even be almost transport-limited. Furthermore, a net deposition of sediments should also be described by the transport-limited version of the model ($K_d \to \infty$).

Alternatively, the shared stream-power model can be written in the form

$$E = \frac{K_d}{K_t A}(Q_c - Q), \tag{12}$$

which closes the loop to the idea of the undercapacity model proposed by Kooi and Beaumont (1994). This model starts from the transport-limited regime instead of the SPIM and attributes erosion and deposition to the deviation of the actual sediment flux Q from the transport capacity Q_c. The almost symmetric formulation of the shared stream-power model in Equation 11 emphasizes the equivalence of both starting points.

The mathematical equivalence of the shared stream-power model to the ξ-q model is recognized by defining $K = K_d$ and $G = \frac{K_d}{K_t}$. However, it should be emphasized that this definition of G as a ratio of two erodibilities is in its spirit fundamentally different from the original definition based on settling velocities. So there is a process-related interpretation of the parameter G and a generic interpretation. While Davy and Lague (2009) estimated $G \gtrapprox 1$ from typical settling velocities, the more recent study of Guerit et al. (2019) used natural and experimental river profiles for estimating G. So the idea of estimating G by its effect on topography rather than from its ingredients was already present before the shared stream-power model and the generic interpretation $G = \frac{K_d}{K_t}$ were proposed. In the following, the generic interpretation is used without introducing a new symbol in order emphasize that the estimates of G given by Guerit et al. (2019) and future estimates derived from topography are valid for the definition $G = \frac{K_d}{K_t}$.

The motivation for replacing the symbol K from the other models (SPIM, linear decline model, ξ-q model) by K_d in the shared stream-power model may not be obvious. In this context, it has to be taken into account that values of K are typically not derived from theoretical considerations, but inferred from field data, for example, recently in a comprehensive compilation of worldwide basin-averaged denudation rates by Harel et al. (2016). For spatially uniform erosion, the sediment flux is $Q = EA$, and Equation 11 collapses to a form analogous to the SPIM (Equation 1) with an effective erodibility K according to

$$\frac{1}{K} = \frac{1}{K_d} + \frac{1}{K_t}. \tag{13}$$

This means that relating measured erosion rates to catchment sizes and channel slopes does typically not yield K_d (so K of the other models), but rather the effective erodibility K according to Equation 13 (in the best case of spatially uniform erosion). So, if we see Equation 1 not as the SPIM (detachment-limited erosion), but as an expression for spatially uniform erosion in the respective upstream catchment, the effective erodibility K according to Equation 13 is the relevant property. Therefore, it makes sense to reserve the symbol K for this property and introduce a new symbol K_d for the erodibility in absence of transported sediment.

As an alternative to Equation 11, the shared-stream power model can be written in terms of K and $G = \frac{K_d}{K_t}$:

$$\frac{1}{1+G} E + \frac{G}{1+G} \frac{Q}{A} = K A^m S^n = K \left(\frac{\partial H}{\partial \chi} \right)^n \tag{14}$$

In the sense of sharing stream power, a fraction $\frac{1}{1+G}$ of the total stream power is spent for incision, while a fraction $\frac{G}{1+G}$ is spent for sediment transport at uniform erosion ($Q = EA$). Alternatively, we can also say

$$\frac{Q}{Q_c} = \frac{K}{K_t} = \frac{G}{1+G}. \tag{15}$$

With regard to Equations 14 and 15, introducing a new parameter $\Gamma = \frac{G}{1+G} \in [0, 1]$ might be convenient since it directly corresponds to the fraction of stream power used for sediment transport or to the ratio of the actual sediment flux and the transport capacity at uniform erosion. However, the parameter G has the same value of G in the ξ-q model, where some preliminary estimates have already been obtained from analyzing natural and experimental river profiles (Guerit et al., 2019). So it might be better to keep G in this context.

Which form of the shared stream-power model (Equations 11 or 14) is more suitable, depends on the question. The K-G version (Equation 14) has the advantage that K is directly related to the steepness of river profiles at uniform erosion. It mainly defines how steep topographies will be at a given uplift rate, so that it is not a big challenge to find a realistic estimate for a given scenario. In turn, G allows for moving between the SPIM and the fully transport-limited model without changing equilibrium topographies fundamentally.

The K_d-K_t version (Equation 11) is particularly useful if considering spatial variations, for instance in lithology. Then the simplest concept would be assuming that K_d directly depends on the properties of the bedrock (or of deposited sediments), while K_t might even be independent of the lithology. This version should also be preferred for extensions of the model. As an example, assuming that a given fraction of the detached material is swept out of the system as dissolved load could be included easily by increasing K_t accordingly. In turn, assuming that K_d increases with Q would be an option to include the tools effect.

3. Scope

While the shared stream-power model covers the entire range from detachment-limited to transport-limited erosion, both end-members differ fundamentally concerning their mathematical properties. As discussed above, the SPIM is described by a hyperbolic differential equation of the advection type, where knickpoints propagate upstream. In turn, the transport-limited end-member follows a parabolic differential equation of the diffusion type where mobile knickpoints cannot exist. This behavior is immediately recognized by setting $K_d \to \infty$ in Equation 11. While discontinuities in E go along with slope-break knickpoints (discontinuities in S) in the general model, the first term vanishes for $K_d \to \infty$, so knickpoints can only arise from discontinuities in Q or A (at confluences) or in K_t.

This leads us to the central question of this study. How do knickpoints behave in the regime between the two extremes of the SPIM and transport-limited erosion? In particular, are mobile knickpoints smoothed by sediment transport, and how does their lifetime depend on the parameters? At one side, these properties are fundamental for the question of how well knickpoints can be detected in reality and over which time spans they can be used for recording the tectonic or climatic history. In turn, the prevalence or absence of knickpoints could provide insights into the relevance of sediment transport for landform evolution even in rivers with little alluvial cover.

The transition from an advection equation to a diffusion equation might suggest that the mixed model behaves like a diffusion-advection equation where knickpoints migrate upstream, but are smoothed through time. However, Gasparini et al. (2006, 2007) already found a two-phase response of the linear decline model and of some more elaborate models to disturbances, where the behavior is initially similar to the SPIM, but turns into a more diffusive behavior later. At that time, however, results were limited by computing capacities as well as by the performance of the available numerical schemes. It seems that the question has not been addressed systematically since then, although simulations on lattices of several million nodes can be run over long time spans nowadays.

This study is not intended to cover the variety of phenomena in the context of knickpoints, where already only a few were discussed in Section 1. Focus is on the simplest scenario of tectonic knickpoints, slope-break knickpoints at vertical faults (Figure 1a). As discussed in Section 1, vertical-step knickpoints (Figure 1b) can be conceptually described as a pair of slope-break knickpoints. However, neither the SPIM nor its extensions were designed for application to very steep slope segments. So the results of the following sections may also be helpful for understanding the effect of sediment transport on vertical-step knickpoints, but these are not considered explicitly.

Concerning the effect of sediment transport on erosion, this study is also reduced to a minimum, represented by the shared stream-power model. In particular, the tools effect of the sediment flux is not taken into account. Both formulations of the model (K_d-K_t, Equation 11 or K-G, Equation 14) would be suitable for covering the range from the SPIM to a transport-limited model. In terms of K_d and K_t, we could assume that K_t is constant, while K_d refers to the properties of the bedrock. Increasing K_d, so assuming a more erodible bedrock, would be a shift to-

ward the transport-limited model. In the following, however, the *K*-*G* version with fixed K and variable G is used. This means that we compare conditions where all rivers would have the same equilibrium profile under uniform uplift, while increasing $G = \frac{K_d}{K_t}$ moves toward the transport-limited model.

4. Model Setup

This study combines analytical considerations with the results of numerical simulations, starting from the linear version ($n = 1$) of the shared stream-power model with $\theta = 0.5$. Since the physical dimension of K (and also K_d and K_t) is time^{-1} then, the erodibility directly defines the time scale of the model, regardless of the spatial scale. As an order of magnitude, we may follow Robl et al. (2017) and assume $K = 2.5$ Myr^{-1}. Then, one time unit corresponds to a time scale $\tau = \frac{1}{K} = 400,000$ yr, regardless of the spatial scale.

The linear model with $\theta = 0.5$ is even invariant under horizontal scaling since the occurrences of the horizontal length scale in the catchment size and in the channel slope compensate each other. While this invariance was seen as an unrealistic property of the SPIM by Kwang and Parker (2017), it only reflects the property $S \to \infty$ for $A \to 0$ if hillslope processes are not taken into account, which leads to a dependence of relief on the mesh width of the considered grid (e.g., Hergarten, 2020a). This problem is independent of θ and requires a thorough consideration of the spatial resolution, but is not an argument against the choice $\theta = 0.5$.

In the following, a fluvial equilibrium topography for uniform uplift (the same as in Hergarten, 2020b, 2021b) on a 5,000 × 5,000 grid is used as an initial topography. Nondimensional coordinates are used, where the pixel size defines the horizontal length scale. The vertical length scale is defined by assuming $K = 1$ and a uniform uplift rate $U = U_0 = 1$. While the topography was computed using the SPIM, it is a valid equilibrium topography for any combination of K_d and K_t that satisfy Equation 13 with $K = 1$ since K and U_0 are constant.

In all examples, it is assumed that the uplift rate suddenly changes from $U = U_0$ to $U = U_0 + u$ at $t = 0$ in the central part of the domain, $1,000 \le x_2 \le 4,000$. This region of increased (or reduced) uplift was extended in such a way that it includes the entire upstream catchment of each point. The boundary of the region of increased uplift is depicted by the red lines in Figure 2.

It was assumed that the change in uplift u is so small that it will not cause changes in the flow pattern. While the reorganization of drainage patterns was addressed in several studies (e.g., Castelltort et al., 2012; Hergarten & Neugebauer, 2001; Lyons et al., 2020; Willett et al., 2014), including their effect in the simulations would not be helpful for understanding the fundamental properties of knickpoints.

In the following, the symbols H_0, U_0, E_0, and Q_0 refer to the initial steady-state topography. The respective lowercase symbols refer the time-dependent deviations from this state arising from the change u in uplift, so that, for example, $H = H_0 + h$ is the time-dependent surface elevation.

Subtracting the respective version of Equation 11 for H and for H_0 yields

$$\frac{e}{K_d} + \frac{q}{K_t A} = \left(\frac{\partial H_0}{\partial \chi} + \frac{\partial h}{\partial \chi}\right)^n - \left(\frac{\partial H_0}{\partial \chi}\right)^n, \tag{16}$$

where

$$e = u - \frac{\partial h}{\partial t}, \tag{17}$$

and q is the integral of e over the upstream catchment. For the linear model ($n = 1$), Equation 16 reduces to

$$\frac{e}{K_d} + \frac{q}{K_t A} = \frac{\partial h}{\partial \chi}, \tag{18}$$

which means that h, q, and e are described by the same equation as H, Q, and E, respectively (Equation 11 for $n = 1$). Inserting Equation 17 into Equation 18 also reveals that h, e, and q are directly proportional to u.

This linearity simplifies both the numerical implementation and the formulation of theoretical relations. Instead of using the equilibrium topography as an initial state, we can set $H_0 = 0$ everywhere (so only use the drainage

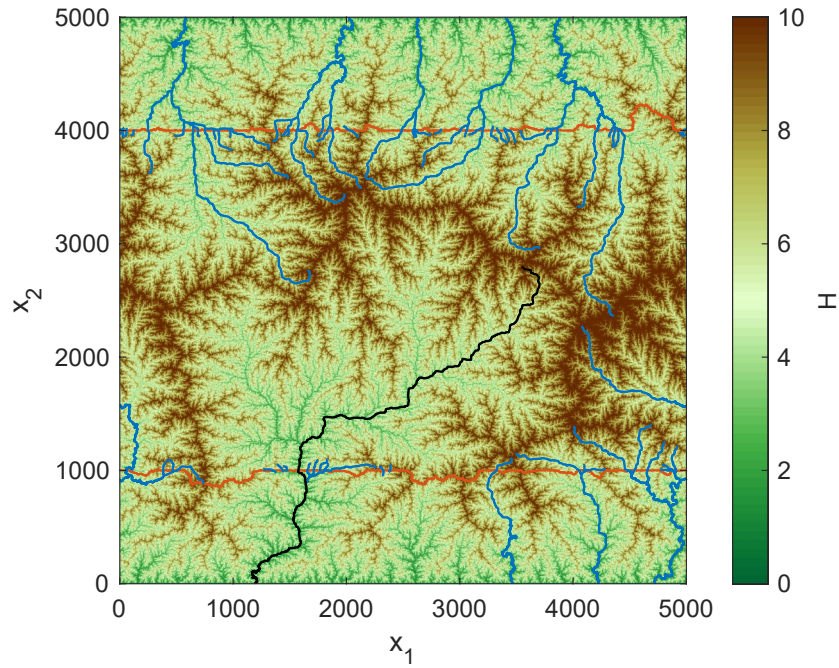

Figure 2. Equilibrium topography used as an initial state. The red lines depict the boundary of the region of increased uplift. The blue and black lines show the rivers investigated in detail, where the black line refers to the river considered in Figures 3, 4, 10 and 11.

pattern of the original topography) and assume $U = 1$ for $1{,}000 \leq x_2 \leq 4{,}000$ and $U = 0$ outside this region. Then, the computed topography H at time t is not an absolute elevation, but the change in surface elevation per change in uplift rate, $\frac{h}{u}$. The same holds for the erosion rate and for the sediment flux. This treatment also covers negative changes in uplift rate $u < 0$, which means that a decrease $-u$ in uplift has the same effect on h as an increase u, except for the sign.

5. Qualitative Analysis

As a first example, Figure 3 shows the evolution of the largest river in the domain (black line in Figure 2) for the SPIM, where $U_0 = u = 1$. For illustration, it refers to the full elevation $H = H_0 + h$ and not to the change in elevation h as described in the previous section.

It is immediately recognized that the velocity of knickpoint migration with regard to the along-stream coordinate x is not constant, but decreases while the knickpoint migrates upstream. With regard to the vertical axis, however, the rate of migration is constant. This fundamental property was described first by Whipple and Tucker (1999) and will be revisited in Section 11. In this scenario, the knickpoint moves upward by 2 vertical units within 1 time unit. So the rate is equal to the uplift rate $U = U_0 + u = 2$. We could also say that the knickpoint follows the uplifted rock vertically. However, this property relies on the specific condition of equilibrium under uniform uplift. So its value for developing a general framework is limited.

After applying the χ transform, river segments exposed to uniform erosion turn into straight lines, and the knickpoint moves along the χ axis at a constant velocity. As pointed out by Royden and Perron (2013), this is a general property of the linear model ($n = 1$) and does not rely on any specific conditions.

Therefore, χ-transformed profiles will be used in the following, where the origin of the χ-axis is set to the stationary knickpoint (intersection with the red lines in Figure 2, red dot in Figure 3). In addition, only the change in elevation h as described in the previous section is considered, so that the initial state is characterized by $h = 0$. Figure 4 shows the respective evolution of the largest river for $G = 0$ (SPIM, $K_d = 1$, $K_t = \infty$), $G = 1$ ($K_d = 2$, $K_t = 2$), and $G = \infty$ (transport-limited, $K_d = \infty$, $K_t = 1$).

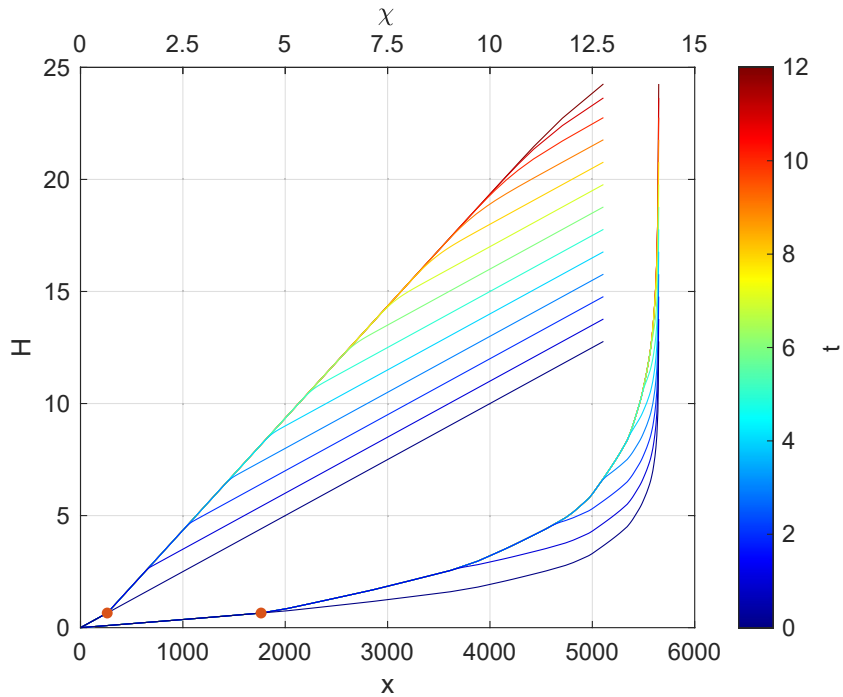

Figure 3. Evolution of the largest river in the domain (black line in Figure 2) for the SPIM, plotted at equal time increments $\delta t = 1$, where $U_0 = u = 1$. The lower set of lines refers to the original river profile, where the origin of the along-stream coordinate x is at the boundary of the domain. The upper set of lines describes the respective χ-transformed profiles. The red dots mark the location of the stationary knickpoint at the fault.

While the profiles for $G = 0$ are basically the same as those shown in Figure 3, the representation in Figure 4 is more general. Formally, it describes the change in elevation for $u = 1$, but as discussed in Section 4, the plot for any change u in uplift is obtained by multiplying h by u, which would also hold for $u < 0$ (a decrease in uplift rate). As expected, a mobile knickpoint moves upstream at a velocity $K_d = 1$ for the SPIM ($G = 0$). The river segment between the stationary knickpoint at $\chi = 0$ and the mobile knickpoint has a steepness index $\frac{\partial h}{\partial \chi} = u = 1$. The region above the mobile knickpoint just follows the increased uplift without any changes in channel steepness ($\frac{\partial h}{\partial \chi} = 0$).

The results for the shared stream-power model with $G = 1$ are qualitatively similar to the SPIM at short times, but the river segment between the stationary knickpoint and the mobile knickpoint is less steep. In turn, the mobile knickpoint moves faster. After the mobile knickpoint has left the domain at $t \approx 6$, the river still becomes steeper

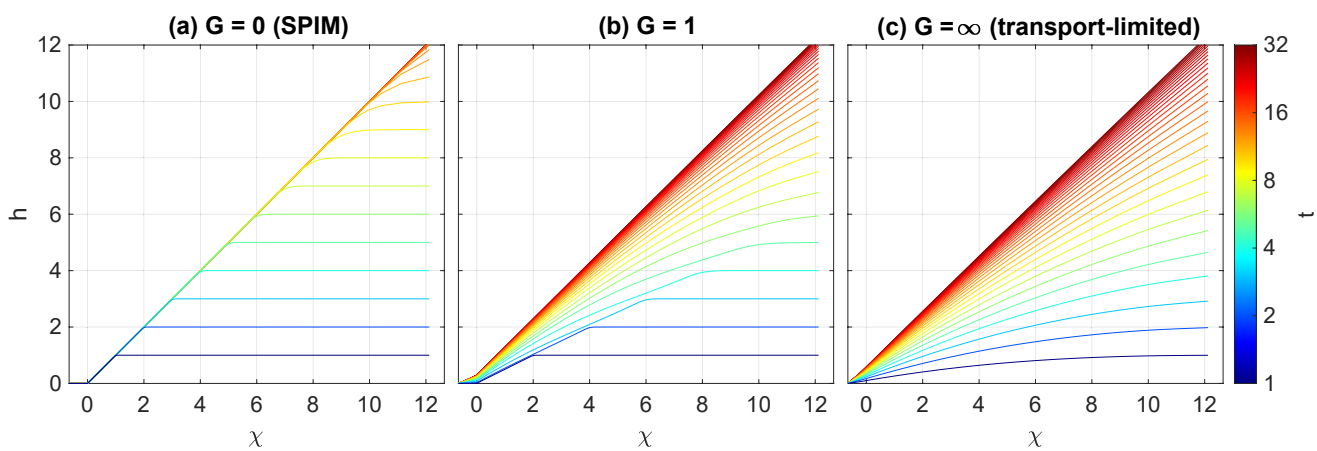

Figure 4. River profiles of the largest river for $G = 0$, $G = 1$, and $G = \infty$ in χ representation. The origin of the χ-axis is set to the stationary knickpoint. Profiles are plotted at equal time increments $\delta t = 1$.

until it finally approaches the same equilibrium steepness as in the SPIM ($\frac{\partial h}{\partial \chi} = 1$). The transport-limited model ($G = \infty$) approaches the same equilibrium steepness without any distinct knickpoints.

It is already visible that the shared stream-power model is not a combination of the advection-type equation of the SPIM with the diffusion-type equation of the transport-limited model to an advection-diffusion equation. In this case, the mobile knickpoint should simply be smoothed while migrating upstream. Instead, the evolution rather consists of two different phases. In the beginning, it is similar to the SPIM, which means that sediment transport plays a minor part. Later, sediment transport becomes increasingly important, and the evolution is similar to the transport-limited end member. While a similar behavior was already found by Gasparini et al. (2006, 2007) in the linear decline model and in some more elaborate models, a quantitative analysis and the development of the theory is the subject of the following sections.

6. Mobile Knickpoints

The numerical analysis of mobile knickpoints is hampered by numerical diffusion. Figure 4a reveals that the mobile knickpoint is more and more smoothed as it moves upstream in the SPIM, while the sharp edge should theoretically persist until the knickpoint arrives at the drainage divide (e.g., Royden & Perron, 2013). The conversion of a distinct knickpoint into a zone with a gradual change in steepness is called knickpoint smearing or knickpoint stretching.

Numerical diffusion is an inherent property of the first-order scheme used for computing the channel slope and affects explicit and implicit schemes in a similar way. A higher-order scheme that reduces numerical diffusion was proposed by Campforts and Govers (2015) and implemented in the landform evolution model TTLEM (Campforts et al., 2017). However, such higher-order schemes are not compatible with implicit schemes. As discussed by Hergarten (2020b), sediment transport reduces the maximum stable time increment of explicit schemes extremely. So it seems to be impossible to avoid the numerical diffusion at a reasonable effort.

Practically, however, numerical diffusion is not as severe as it looks in Figure 4 since the χ transform is highly nonlinear and stretches the upper segments of rivers. While the mobile knickpoint appears to be strongly smoothed when it passes the middle of the χ axis ($\chi \approx 6$) in Figure 4a, Figure 3 reveals that is point is already close to the drainage divide in the original river profile. So only the uppermost river segments are seriously affected by knickpoint smearing due to numerical diffusion.

Nevertheless, knickpoint smearing still hampers a thorough investigation of the properties of the knickpoints. So let us start with a theoretical investigation by applying the method of characteristics to Equation 18 in combination with Equation 17. This method considers the topography not at a given position as a function of time, but along lines $\chi(t)$. So we would move along a river profile that changes through time along a suitable path $\chi(t)$, where we will recognize in the next step what suitable means. The rate of change in $h(\chi(t), t)$ along any path $\chi(t)$ is given by the total derivative

$$\frac{dh}{dt} = \frac{\partial h}{\partial \chi}\frac{d\chi}{dt} + \frac{\partial h}{\partial t} \tag{19}$$

$$= \left(\frac{u - \frac{\partial h}{\partial t}}{K_\mathrm{d}} + \frac{q}{K_\mathrm{t} A} \right) \frac{d\chi}{dt} + \frac{\partial h}{\partial t}. \tag{20}$$

The partial derivative $\frac{\partial h}{\partial t}$, so how h changes through time at a fixed position, is not immediately known. So a path $\chi(t)$ is suitable for simplifying the problem if $\frac{\partial h}{\partial t}$ vanishes from the equation, which is the case here if $\chi(t)$ satisfies the condition

$$\frac{d\chi}{dt} = K_\mathrm{d}. \tag{21}$$

The respective paths $\chi(t)$ starting from different points $\chi(0)$ at $t = 0$ are the so-called characteristics of the differential equation. Here, the characteristics move upstream along the χ-axis at a velocity K_d. Since this velocity

is constant and the same for all characteristics, the method of characteristics is equivalent to using a coordinate system that moves upstream at a constant velocity K_d here. Equation 20 turns into

$$\frac{dh}{dt} = u + \frac{K_d}{K_t}\frac{q}{A} \tag{22}$$

then. Without the second term, characteristics starting from different points $\chi(0)$ would be decoupled, which means that h along each characteristic can be computed without knowing anything about the neighborhood, so about the other characteristics. Then, Equation 22 could be solved analytically by

$$h(\chi(t),t) = \int_0^t u(\chi(\tau),\tau)\,d\tau = \begin{cases} ut & \chi(t) \geq K_d t \\ \frac{u}{K_d}\chi(t) & \text{for} \quad 0 < \chi(t) < K_d t \\ 0 & \chi(t) < 0 \end{cases} \tag{23}$$

This solution describes a mobile knickpoint migrating upstream at the velocity K_d, where the segment between the stationary knickpoint at $\chi = 0$ and the mobile knickpoint has a constant steepness index $\frac{\partial h}{\partial \chi} = \frac{u}{K_d}$. This solution is the same as for the linear version of the SPIM, but with K_d instead of K.

Since q is the integral of e over the upstream catchment, characteristics are not fully decoupled in the shared stream-power model (Equation 22). The future development along a given characteristic is independent of the downstream characteristics (lower χ), but still depends on the upstream characteristics (higher χ). This residual one-sided coupling impedes a full analytical solution, but helps to constrain the properties of the solution. In particular, the upper part of Equation 23,

$$h = ut \quad \text{for} \quad \chi \geq K_d t, \tag{24}$$

remains valid for the shared stream-power model since $e = 0$ here and thus also $q = 0$. This means that the river segment defined by $\chi > K_d t$ does not change its shape as long as it exists, but is just uplifted uniformly. In particular, there is no upstream knickpoint smearing in the shared stream-power model.

The behavior downstream of the presumed (since it might still be a smooth transition in channel slope) mobile knickpoint at $\chi = K_d t$ is, however, more complicated. Since points below this point (characteristics that start at $\chi(0) < 0$) have already experienced a change in erosion rate ($e > 0$), $q > 0$ there. This increased sediment flux inhibits erosion below the mobile knickpoint. Since it increases downstream, it reduces the channel steepness below the presumed knickpoint. In the following, it will be shown that this effect is not strong enough to remove the difference in k_s across the presumed knickpoint rapidly, in which case the considered point would no longer be a slope-break knickpoint.

According to Equation 18, the additional erosion rate e is constrained by

$$e < K_d \frac{\partial h}{\partial \chi}. \tag{25}$$

This constraint is relevant for the upstream catchment of the considered point up to the presumed mobile knickpoint, while $e = 0$ above this point. This condition constrains the increase in sediment flux q according to

$$q = \int e\,dA \leq \max(e) \int_{e>0} dA, \tag{26}$$

where the integral extends only over the part of the upstream catchment where the erosion rate has already increased, so between the considered point and the presumed mobile knickpoint. If we define

$$\psi = \frac{\int_{e>0} dA}{A} \tag{27}$$

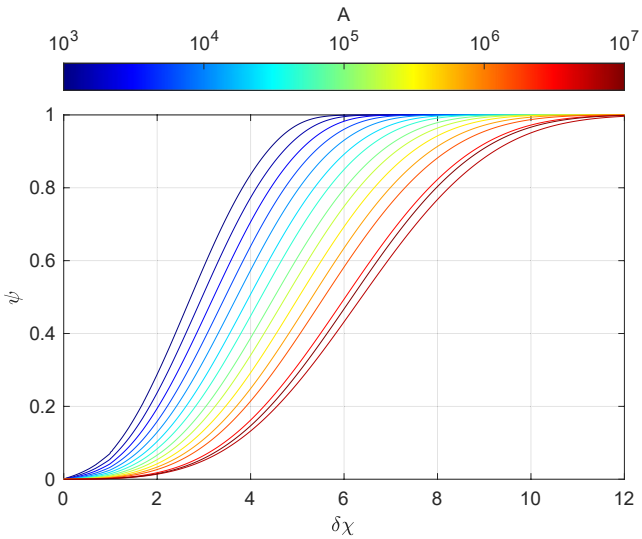

Figure 5. Ratio ψ of the catchment size up to a given value $\delta\chi$ above the considered point to the total upstream catchment size A. The color refers to the total upstream catchment size A. The first curve refers to the mean over all catchments with sizes from 512 to 1,023 pixels, the second curve to 1,024 to 2,047 pixels, etc.

as the respective fraction of the total upstream catchment size A, the ratio $\frac{q}{A}$ occurring in Equation 22 can be constrained by

$$\frac{q}{A} \leq \psi \max(e) < \psi K_\mathrm{d} \max\left(\frac{\partial h}{\partial \chi}\right) \tag{28}$$

according to Equation 25.

The nondimensional factor ψ is plotted in Figure 5, where $\delta\chi$ on the x-axis is the distance between the presumed knickpoint and the considered point on the χ-axis. The factor ψ increases with increasing $\delta\chi$ at a given catchment size A (which is trivial), but decreases with increasing A. Since the χ-transformed equilibrium river profiles are straight lines for uniform uplift, Figure 5 is basically the same as the hypsometric curve on a catchment basis.

Inserting Equation 28 into Equation 22 yields

$$\frac{dh}{dt} < u + \psi \frac{K_\mathrm{d}^2}{K_\mathrm{t}} \max\left(\frac{\partial h}{\partial \chi}\right). \tag{29}$$

Then, the elevation difference δh toward the presumed knickpoint (where $\frac{dh}{dt} = u$) decreases through time, but

$$\frac{d\delta h}{dt} < \psi \frac{K_\mathrm{d}^2}{K_\mathrm{t}} \max\left(\frac{\partial h}{\partial \chi}\right). \tag{30}$$

The occurrence of the $\frac{\partial h}{\partial \chi}$ impedes an instantaneous decrease of δh and thus a decrease of the steepness index $\frac{\partial h}{\partial \chi}$ to zero even for points very close to the presumed knickpoint. So the point at $\chi = K_\mathrm{d} t$ is indeed a sharp knickpoint and not exposed to smearing.

It is noteworthy that the velocity of knickpoint migration along the χ axis is K_d, and the initial change in k_s is $\frac{u}{K_\mathrm{d}}$. So the initial response is dictated by the detachment-limited erodibility K_d. Revisiting Figure 3, the increased velocity at $G = 1$ compared to the SPIM ($G = 0$) arises from keeping the effective erodibility $K = 1$ (Equation 13) constant. Then $G = 1$ requires $K_\mathrm{d} = 2$ instead of $K_\mathrm{d} = 1$ for $G = 0$. If K_d was kept constant and the transition from the SPIM toward the transport-limited model was employed by reducing K_t, the initial response would be the same in Figures 3a and 3b. However, the initial equilibrium topography (which is not visible) and the long-term response would depend on K_t then. In this sense, the increase in knickpoint migration velocity observed in Figure 3 is not a direct effect of sediment transport, but arises from comparing river profiles starting from the same initial profile at the same uplift rate. However, as discussed in Section 2, this should not be seen as an artifact, but is rather the natural approach when analyzing real-world river profiles.

While a distinct break in channel slope persists, the steepness index downstream of the knickpoint gradually decreases through time, and thus also the difference in steepness index across the knickpoint. In order to distinguish this effect from knickpoint smearing, the term knickpoint flattening is used in the following. Since the factor ψ decreases with increasing catchment size, flattening is slower at larger catchment sizes.

Knowing that knickpoint smearing in Figure 4 is solely a numerical artifact, knickpoint flattening can be investigated numerically despite the numerical diffusion. Assuming that numerical diffusion acts almost symmetrically, the slope $\frac{\partial h}{\partial \chi}$ at the knickpoint should be the mean of $\frac{\partial h}{\partial \chi}$ above and below the knickpoint. Since $\frac{\partial h}{\partial \chi} = 0$ above the knickpoint, $\delta k_\mathrm{s} = 2\frac{\partial h}{\partial \chi}$ is an estimate of the difference in the steepness index $\delta k_\mathrm{s} = k_{\mathrm{s}\downarrow} - k_{\mathrm{s}\uparrow}$ (where $\downarrow$ and $\uparrow$ refer to downstream and upstream of the knickpoint, respectively) across the knickpoint. In order to achieve a reasonable accuracy, the slope $\frac{\partial h}{\partial \chi}$ is only computed when the knickpoint passes any node of the grid (so at the time when it is closest to the node according to the χ-coordinate of the node and to the velocity of migration K_d). Then, the node and its upstream and downstream neighbors are interpolated by a parabolic function, and the slope of the parabolic function at the exact position of the knickpoint is computed. This procedure was tested for the SPIM,

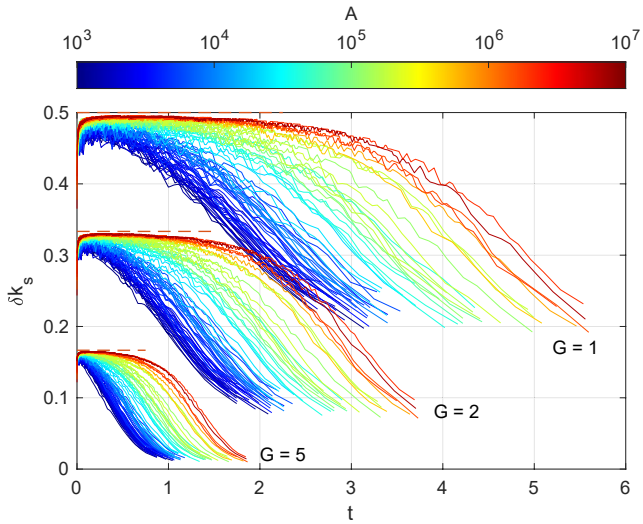

Figure 6. Difference in steepness index across the mobile knickpoint. The color refers to the catchment size A at the stationary knickpoint. The last point of each curve corresponds to the time when the knickpoint passes the second-last point of the river. The dashed red lines show the theoretical initial value $\delta k_s = \frac{1}{K_d}$.

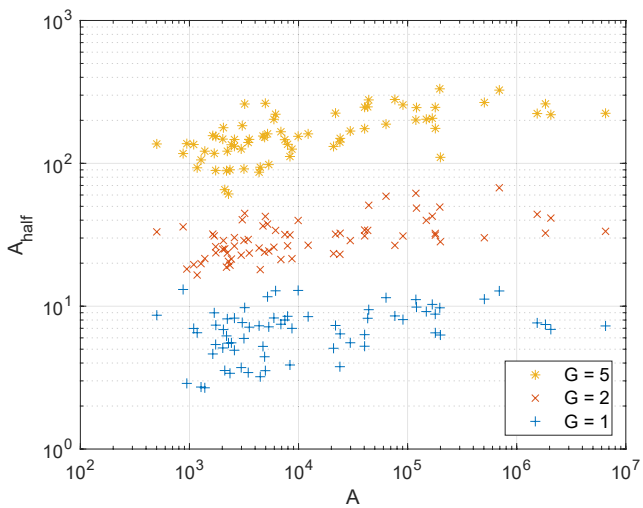

Figure 7. Catchment size A_{half} where the mobile knickpoint has flattened by 50%, that is, where δk_s has decreased to half of its initial value $\frac{1}{K_d}$.

where δk_s should be $\delta k_s = 1$ up to the drainage divides. All obtained values were in the range $0.85 < \delta k_s < 1$. So the scheme still underestimates δk_s by up to 15%, but this is not crucial.

The results shown in Figure 6 reveal that δk_s stays almost constant at $\frac{1}{K_d}$ for some time in large rivers, which is consistent with small values of ψ at small $\delta\chi$ for large catchment sizes. After the knickpoint has migrated upstream for some time, δk_s decreases, where the curves for rivers of different sizes are mainly shifted horizontally. This means that the degree of flattening mainly depends on how long the knickpoint still has to migrate to the drainage divide, which is equivalent to its actual distance to the drainage divide on the χ-axis. Its history, that is, how long it has been migrating, has a minor influence.

In order to quantify the effect of flattening, the catchment size A_{half} where the knickpoint has flattened by 50% was measured, that is, where δk_s across the knickpoint has decreased to half of its initial value $\frac{1}{K_d}$. Figure 7 shows that A_{half} is typically smaller than 10 pixels for $G = 1$. It increases with increasing G, but is not larger than some hundred pixels for $G = 5$. Beyond this, A_{half} depends only weakly on the catchment size A at the stationary knickpoint. This result is in agreement with the previous finding that the degree of flattening mainly depends on the actual position of the knickpoint in relation to the drainage divide, while the distance from the stationary knickpoint has a minor effect.

7. Stationary Knickpoints

A fundamental property of stationary knickpoints is readily obtained by combining Equations 3 and 11 in the form

$$\frac{U - \frac{\partial H}{\partial t}}{K_d} + \frac{Q}{K_t A} = \left(\frac{\partial H}{\partial \chi}\right)^n = k_s^n. \tag{31}$$

Both the rate of change in surface elevation $\frac{\partial H}{\partial t}$ and the sediment flux Q must be continuous across the knickpoint, while the uplift rate U is discontinuous and makes a step of u. So this discontinuity must be directly reflected in a jump of the steepness index (i.e., a slope-break knickpoint) according to

$$k_{s\uparrow}^n - k_{s\downarrow}^n = \frac{u}{K_d}. \tag{32}$$

This difference is basically the same as in the SPIM without sediment transport. Similar to the velocity of knickpoint migration, the only difference is that the erodibility is not the effective erodibility K (Equation 13), but K_d.

For the linear version, Equation 32 implies that the difference $k_{s\uparrow} - k_{s\downarrow}$ across the knickpoint is constant, while both $k_{s\uparrow}$ and $k_{s\downarrow}$ increase through time for $u > 0$. In terms of knickpoint flattening as discussed in Section 6, this means that the stationary knickpoint is not flattened absolutely, but only relative to the overall channel steepness around the knickpoint. In turn, Equation 32 predicts a decrease in $k_{s\uparrow} - k_{s\downarrow}$ for $n > 1$, so an absolute flattening of the knickpoint. This flattening, however, should not affect the ability to detect stationary knickpoints fundamentally.

However, there seems to be no analytical solution for $k_{s\uparrow}$ and $k_{s\downarrow}$ as a function of time. Figure 8 shows $k_{s\uparrow}$ for the 69 rivers obtained from numerical

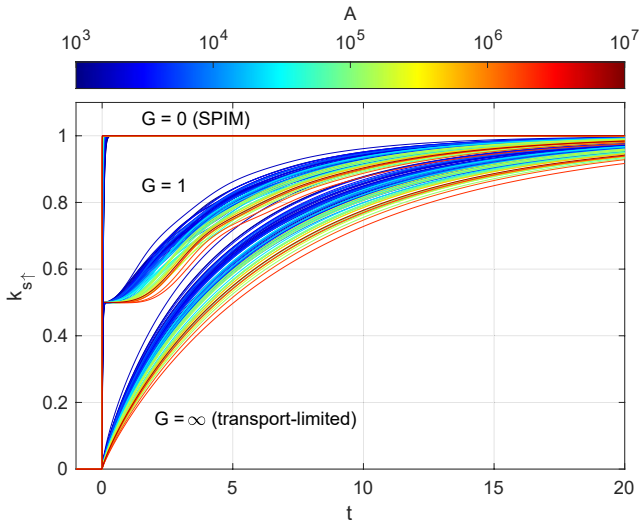

Figure 8. Steepness index upstream of the stationary knickpoint (relative to the steady-state topography) for $G = 0$ (SPIM), $G = 1$, and $G = \infty$. The color refers to the catchment size A at the stationary knickpoint.

solutions for $G = 1$ and for the transport-limited model ($G = \infty$). The result obtained from the SPIM ($G = 0$) was included for comparison, where a step-like adjustment from $k_{s\uparrow} = 0$ to 1 should occur theoretically. For $G > 0$, the adjustment toward the asymptotic value $k_{s\uparrow} \to 1$ is faster for small rivers (blue curves). While this result is not surprising, it is visible that even a variation in A over some orders of magnitude results in a moderate change in the time scale of adjustment.

The curves for $G = 1$ are qualitatively similar to those in Figure 5, which show the fraction of the upstream catchment size that already delivers more sediment according to the actual position of the mobile knickpoint. In particular, the curves for different catchment sizes differ by some kind of lag in the sense that $k_{s\uparrow}$ and thus also $k_{s\downarrow}$ stay constant for some time for large rivers. This behavior, which was already visible in Figure 4b, is directly related to the result that only a small part of a large catchment is captured by the mobile knickpoint in the beginning.

Figure 9 quantifies the time scale of adjustment as a function of A and G. The time T_{half} when k_s reaches the middle between its initial value and its final value was taken as the characteristic time scale of adjustment. Although the scatter among the 69 rivers is high, a systematic dependence on both A and G is visible. The solid lines are logarithmic functions

$$T_{half} = \alpha \log_{10} A + b \tag{33}$$

fitted for each value of G individually. All obtained values α are between 0.48 and 0.52, where the 95% confidence intervals are considerably wider than this range (the widest interval ranges from 0.4 to 0.6). This result suggests $\alpha = 0.5$.

However, the most important result of Figure 9 is the weak dependence of T_{half} on G. Larger values of G (more toward the transport-limited model) result in a faster adjustment, but the systematic variation over the entire range $G \geq 0.5$ is less than one time unit. So the dependence of T_{half} on both K_d and K_t is weak as long as $K = 1$ as assumed here. Since one time unit is $\frac{1}{K}$ for $\theta = 0.5$, the main dependency of T_{half} is $\frac{1}{K}$. Thus, the time scale of the adjustment of the stationary knickpoint is governed by the effective erodibility K, in contrast to knickpoint migration where K_d defines the velocity. As it is recognized from the straight lines in Figure 9, the systematic variation of T_{half} over the entire range $G \geq 0.5$ and over the four orders of magnitude in catchment size considered here ranges from about 2.8 to 5.8, which is not much more than a factor of two. Using $K = 2.5$ Myr^{-1}, T_{half} is in an order of magnitude of one to a few million years then.

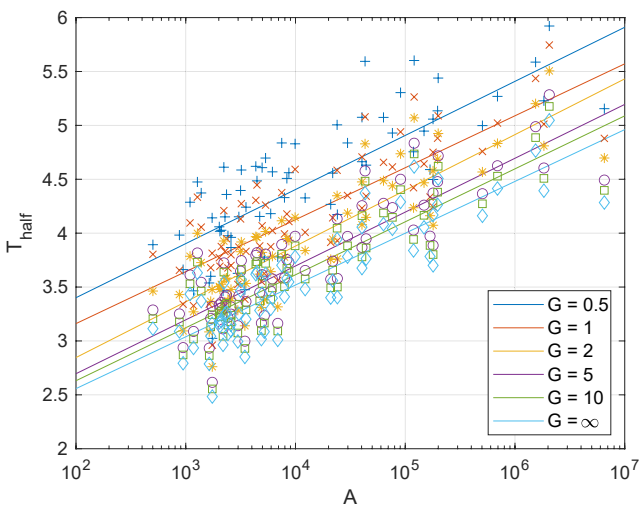

Figure 9. Time T_{half} when k_s reaches the middle between its initial value and its final value as a function of the catchment size A for different values of G. The solid lines are logarithmic functions according to Equation 33.

Let us summarize the findings of the two previous sections and revisit Figure 4. The shared stream-power model (Equation 11) for $n = 1$ can also be interpreted as splitting up the steepness index $k_s = \frac{\partial H}{\partial \chi}$ into a detachment component and a transport component. As the main result of Section 6, the initial response to a tectonic signal only concerns the detachment component. So the steepness index changes by $\frac{u}{K_d}$ at first. This change goes along with the occurrence of a mobile knickpoint, which moves upstream at the velocity $K_d > K$. The second phase of the response is related to the change in sediment flux from the upstream range, which finally causes an additional change of $\frac{u}{K_t}$ in the steepness index. In total, the change is $\frac{u}{K}$. In the SPIM, only the first phase occurs, while the transport-limited end-member shows the second phase only.

Considering the channel steepness at a given point, for example, $\chi = 5$ in Figure 4b, reveals a quite complex behavior of the channel steepness. The steepness suddenly increases when the knickpoint passes. Afterward, the sediment flux increases, which results in a decrease in steepness at first. According

to the findings of Section 6, this decrease is stronger if the upstream catchment is small. Later on, the steepness increases again and approaches the equilibrium steepness dictated by U and K.

8. The Influence of the Spatial Resolution

Both the SPIM and the shared stream-power model do not involve a canonical horizontal length scale. Since the pixel size defines the horizontal length scale in the setup used in this study, all results that involve lengths or areas depend on the spatial resolution of the grid. This concerns the time scale T_{half} of adjustment of stationary knickpoints, which has at least a weak dependency on the catchment size, and the catchment size A_{half} where mobile knickpoints have flattened by 50%.

In the context of T_{half} and A_{half}, the time scale at which sediment transport reacts to changes in base level is the relevant property. This is obvious for the stationary knickpoint, where the sediment flux increases after the change in erosion rate has captured a considerable part of the upstream catchment. As found in Section 7, the response of small catchments is faster than that of large catchments. The same holds for the flattening of mobile knickpoints. While the knickpoint moves upstream, tributaries experience a lowering in base level and respond by an increased sediment flux. Since the response of small catchments is faster, small tributaries have a strong effect on knickpoint flattening.

The pixel size defines the smallest catchment resolved in the model and thus the fastest response to changes in base level. For a single-pixel catchment, the sediment flux is $Q = EA$. Then, the shared stream-power model (Equation 11) collapses to a form analogous to the SPIM (Equation 1) with the effective erodibility K (Equation 13), and the sediment flux is

$$Q = KA^{m+1}S^n. \tag{34}$$

So the sediment flux is a function of the difference of surface elevation and base level via the channel slope S. This means that the delay in the response of the sediment flux to changes in base level vanishes for single-pixel catchments.

In this sense, the pixel size defines the scale where the sediment flux instantaneously responds to changes in base level. This scale should be related to the transition from channelized flow to hillslope processes. A similar interpretation was recently proposed by Hergarten (2020a) for the scaling problem that occurs when the SPIM is coupled to a model for hillslope processes, while previous studies (Howard, 1994; Pelletier, 2010; Perron et al., 2008) attributed the problem to the channel width.

However, some caution is still required since the pixel size does not only define a scale, but also how fast the response is. For the linear model, it is easily recognized that a single-pixel catchment turns into a linear reservoir with a decay constant $\frac{KA^\theta}{\delta x}$, where δx is the distance between the considered point and its flow target. If we, however, assume the transition to any model for hillslope processes (e.g., diffusion), there is no reason why hillslopes should have the same decay constant as single-pixel catchments in the shared stream-power model. So it can only be stated that all occurrences of catchment sizes in T_{half} and A_{half} must be interpreted in terms of a given scale (an area) that is somehow related to the transition from the fluvial regime to hillslope processes, but estimating this scale requires a model for hillslope processes and is nontrivial.

9. The Influence of the Concavity Index

As discussed earlier, the choice $\theta = 0.5$ is convenient for converting nondimensional coordinates to physical coordinates, but several authors prefer a slightly lower reference value $\theta = 0.45$. In order to investigate the effect of the concavity index θ, simulations were also performed with $\theta = 0.4$, where the same drainage network as for $\theta = 0.5$ was used for simplicity.

The equilibrium topography, however, depends strongly on θ. Since catchment sizes are measured in pixels, the values A^θ are lower for $\theta = 0.4$ than for $\theta = 0.5$, in particular for large catchment sizes. The maximum χ value of the largest river above the stationary knickpoint is about 29 for $\theta = 0.4$, while it was about 12 for $\theta = 0.5$, which is an increase by a factor of about 2.5. Since $K = 1$ and $U_0 = 1$ are also assumed here, the maximum surface

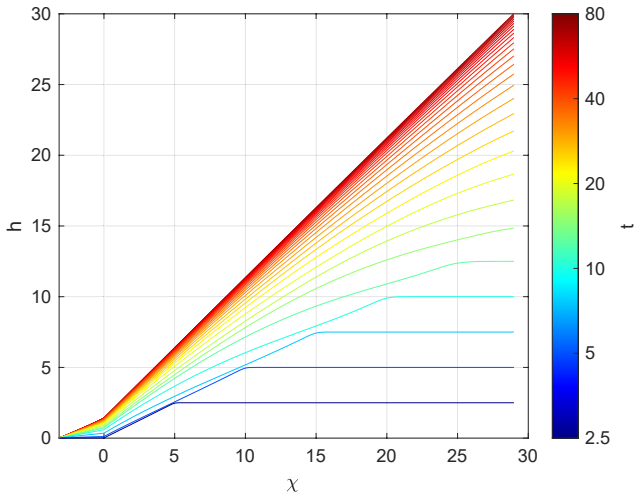

Figure 10. River profiles of the largest river for $\theta = 0.4$ and $G = 1$. The origin of the χ-axis is set to the stationary knickpoint. Profiles are plotted at equal time increments $\delta t = 2.5$.

elevation and the time scale are also larger by this factor. Accordingly, the χ-transformed profiles are plotted at time increments $\delta t = 2.5$ in Figure 10 instead of $\delta t = 1$ in Figure 4.

When comparing Figures 4b and 10, it is recognized that the results for $\theta = 0.4$ are very close to the results for $\theta = 0.5$ except for the scaling. In principle, the relation between A and χ for the individual rivers depends on θ, and thus also the ratio $\frac{Q}{A}$ in Equation 11. However, the effect appears to be small. So the results suggest that there is little influence of the concavity index at least in the range $\theta \in [0.4, 0.5]$.

10. The Nonlinear Model

As discussed in Section 1, there is still uncertainty about the exponent n. The linear model ($n = 1$) is a convenient choice, but recent studies (Adams et al., 2020; Harel et al., 2016; Hilley et al., 2019) rather suggest $n > 1$. As the main complication toward the linear model, the disturbance h in topography cannot be separated from the initial topography H_0 for $n \neq 1$, which was the basis of all considerations of mobile knickpoints in the previous sections. So the properties of knickpoints are no longer independent of the initial topography. This becomes obvious if we try to apply the methods of characteristics (Section 6) to the nonlinear model. Performing the steps from Equations 19–21 for the full shared stream-power model (Equation 11), we obtain

$$\frac{d\chi}{dt} = K_\mathrm{d}\left(\frac{\partial H}{\partial \chi}\right)^{n-1}. \tag{35}$$

So the velocity at which the characteristics move upstream depends on the unknown surface elevation H. Thus, the problem cannot be separated into a first step of computing the characteristics and a second step of computing the elevation along the characteristics. We can, however, at least guess that a straight (H vs. χ) river segment migrates upstream (as a morphologic element, not by material) at a velocity given by Equation 35. Then, steep river segments migrate faster than less steep river segments for $n > 1$. As a consequence, steeper river segments catch up with less steep river segments running ahead, which consumes the adjacent edges of the segments. This process counteracts a potential smearing of convex knickpoints and may even convert convex river segments into knickpoints. So it is called knickpoint sharpening in the following. In turn, concave knickpoints are stretched to an extended transition zone. The behavior for $n < 1$ is opposite. The concept of sharpening and stretching knickpoints and its implications for the velocities of knickpoint migration are described in detail by Royden and Perron (2013) for the SPIM, so that we focus on the new aspects arising from sediment transport.

As a second complication, the change in topography h resulting from different changes in uplift rate u cannot be obtained by rescaling h. In particular, increases and decreases in uplift rate may even have qualitatively different effects as already pointed out by Royden and Perron (2013) for the SPIM.

Let us start with the linearized version of the model. If the change in uplift u is sufficiently small, the right-hand side of Equation 16 can be approximated by

$$\left(\frac{\partial H_0}{\partial \chi} + \frac{\partial h}{\partial \chi}\right)^n - \left(\frac{\partial H_0}{\partial \chi}\right)^n \approx n\left(\frac{\partial H_0}{\partial \chi}\right)^{n-1}\frac{\partial h}{\partial \chi}, \tag{36}$$

so that

$$\frac{e}{K_\mathrm{d}} + \frac{q}{K_\mathrm{t} A} = n\left(\frac{\partial H_0}{\partial \chi}\right)^{n-1}\frac{\partial h}{\partial \chi}. \tag{37}$$

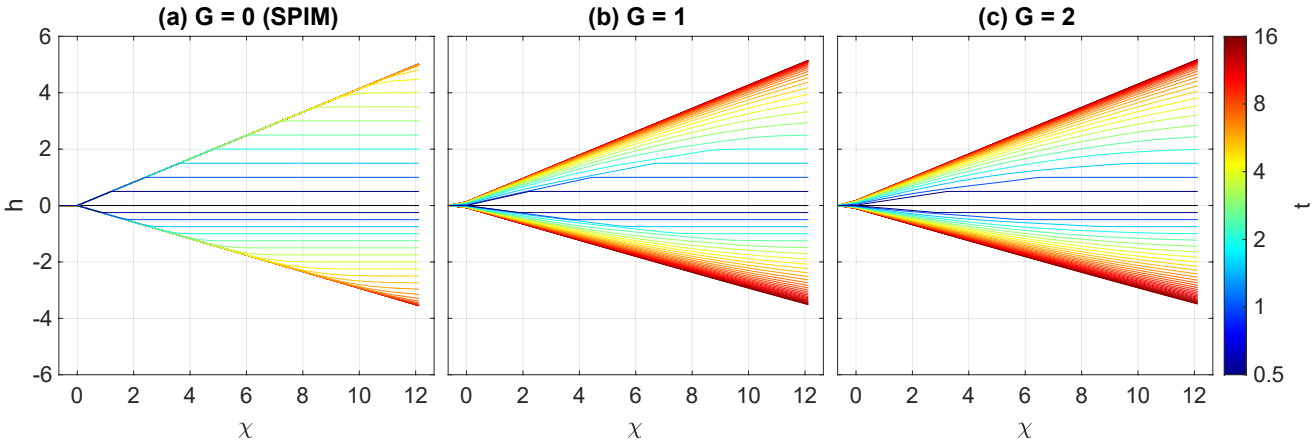

Figure 11. River profiles of the largest river for the nonlinear model with $n = 2$. For clarity, the difference in elevation h toward the equilibrium elevation H_0 is plotted instead of the absolute elevation H. The origin of the χ-axis is set to the stationary knickpoint. Profiles are plotted at equal time increments $\delta t = 0.5$. The upper curves ($h > 0$) refer to an increase in uplift by $u = 1$, and the lower curves ($h < 0$) to a decrease by $u = -0.5$.

This is the same relation as Equation 18 for the linear model except for the term $n(\frac{\partial H_0}{\partial \chi})^{n-1}$. So we can also interpret the linearized model as a linear model where the erodibilities are $nK_d(\frac{\partial H_0}{\partial \chi})^{n-1}$ and $nK_t(\frac{\partial H_0}{\partial \chi})^{n-1}$, respectively. As an immediate consequence, the velocity of knickpoint migration is

$$\frac{d\chi}{dt} = nK_d\left(\frac{\partial H_0}{\partial \chi}\right)^{n-1}. \tag{38}$$

This relation differs formally by the occurrence of the factor n from Equation 35. Thus, a small disturbance on a straight (H vs. χ) river segment migrates upstream n times faster than the segment itself. It seems, however, that Equation 35 is occasionally misinterpreted as the velocity of knickpoint migration (e.g., Beckers et al., 2015).

In our scenario where $\frac{\partial H_0}{\partial \chi} = 1$, equilibrium topographies are the same for all n at the same erodibilities. Then, the linearized model is the same as the linear model with erodibilities nK_d and nK_t, respectively, and all results of the previous sections remain valid, but with erodibilities increased by a factor n. The only effects of nonlinearity are a decrease of the time scale by a factor of n, in particular that knickpoints migrate n times faster, and that a given change in uplift rate u has a smaller effect on the topography. This effect of nonlinearity is, however, not a property unique to the shared stream-power model, but also occurs in the SPIM.

However, the simple result that K_d still dictates the velocity of knickpoint migration and that nonlinearity increases the velocity by a factor n only holds for small changes in uplift, so only for knickpoints where the difference in channel steepness across the knickpoint is much smaller than the overall steepness. Since distinct knickpoints in real rivers typically do not satisfy this condition, the effect of nonlinearity beyond the linear approximation deserves attention.

Figure 11 shows two scenarios for $n = 2$. The upper parts of the plots (curves with $h > 0$) refer to an increase in uplift by $u = 1$. So the uplift rate increases from $U_0 = 1$ to $U_0 + u = 2$. In turn, the lower parts of the plots (curves with $h < 0$) refer to a decrease in uplift by $u = -0.5$. So the uplift rate decreases from $U_0 = 1$ to $U_0 + u = 0.5$.

The plots reveal that the nonlinearity affects the velocity of knickpoint migration beyond the linear approximation, where the velocity would be 2, 4, and 6 for $G = 0$, $G = 1$, and $G = 2$, respectively (Equation 38). Knickpoint migration is faster than predicted by Equation 38 for convex knickpoints ($u > 0$) and slower for concave knickpoints ($u < 0$). Since the respective velocities were already derived by Royden and Perron (2013) for the SPIM, only a sketch of the extension by sediment transport is given in the following. As a main result, it will turn out that the effect of nonlinearity beyond the factor n in the velocity can be expressed in terms of a nondimensional parameter

$$\gamma = \frac{K}{K_d}\frac{u}{U_0}, \tag{39}$$

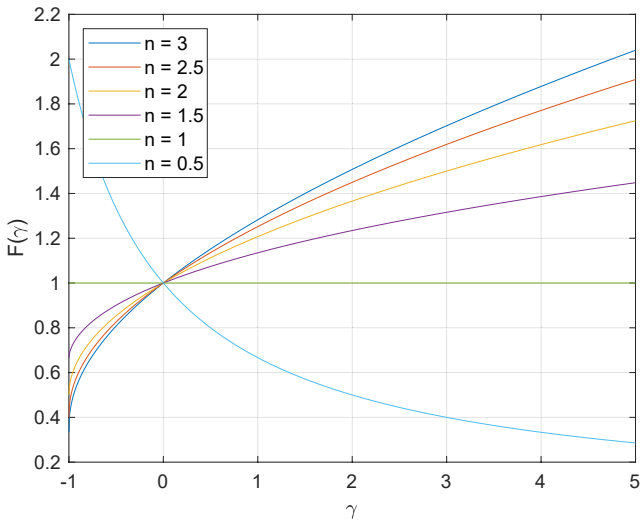

Figure 12. Velocity of knickpoint migration relative to the velocity in the linearized model. The function $F(\gamma)$ (Equation 45) describes the factor by which knickpoints migrate faster than predicted by the linearized model. The nondimensional parameter γ (Equation 39) combines uplift rates and erodibilities.

where the ratio $\frac{u}{U_0}$ (which may be negative) describes the relative strength of the disturbance in uplift, while the first term, $\frac{K}{K_d} \in [0, 1]$, refers to the difference toward the SPIM.

Similar to the linear model, it can be assumed that the change q in the sediment flux is small slightly below the knickpoint, and that uplift is in balance with erosion there. Then, Equation 16 yields

$$\frac{u}{K_d} = \left(\frac{\partial H_0}{\partial \chi} + \frac{\partial h}{\partial \chi}\right)^n - \left(\frac{\partial H_0}{\partial \chi}\right)^n. \tag{40}$$

As described in Section 2, the shared stream-power model collapses to a form analogous to the SPIM with an effective erodibility K according to Equation 13 for spatially uniform erosion. This condition is satisfied for the initial state if U_0 is constant at least within the domain above the knickpoint, and we obtain

$$\left(\frac{\partial H_0}{\partial \chi}\right)^n = \frac{U_0}{K}. \tag{41}$$

Using the nondimensional parameter γ (Equations 39 and 40) can be written in the form

$$\frac{\partial h}{\partial \chi} = \frac{\partial H_0}{\partial \chi}((1+\gamma)^{\frac{1}{n}} - 1). \tag{42}$$

In turn, the river segment above the mobile knickpoint is not affected by any change in erosion, so that $\frac{\partial h}{\partial \chi} = 0$ there. So the river segment below the knickpoint is by the amount given in Equation 42 steeper than the segment above the knickpoint. The latter, however, is still rising at a rate

$$\frac{\partial h}{\partial t} = u, \tag{43}$$

while the lower segment is already in equilibrium ($\frac{\partial h}{\partial t} = 0$). Then the knickpoint, that is, the intersection of the two segments, moves upstream at a velocity

$$\frac{d\chi}{dt} = \frac{\frac{\partial h}{\partial t}}{\frac{\partial h}{\partial \chi}} = \frac{u}{\frac{\partial H_0}{\partial \chi}((1+\gamma)^{\frac{1}{n}} - 1)}. \tag{44}$$

according to Equations 42 and 43. If we define

$$F(\gamma) = \frac{\gamma}{n((1+\gamma)^{\frac{1}{n}} - 1)}, \tag{45}$$

the velocity can be written in the form

$$\frac{d\chi}{dt} = nK_d\left(\frac{\partial H_0}{\partial \chi}\right)^{n-1} F(\gamma). \tag{46}$$

Here, the first terms are the velocity of the linearized version (Equation 38), so in the limit of small changes in uplift, while $F(\gamma)$ describes the effect of nonlinearity. The function $F(\gamma)$ is plotted in Figure 12 for different exponents n.

The result that the effect of nonlinearity can be expressed by the nondimensional parameter γ (Equation 39) is, however, more important than the exact shape of the respective function $F(\gamma)$. While $\gamma = \frac{u}{U_0}$ for the SPIM, it is by a factor of $\frac{K}{K_d} = \frac{1}{1+G}$ smaller in the shared stream-power model, leading to a smaller effect of nonlinearity on the velocity of knickpoint migration. For the examples shown in Figure 11, the velocities are 2.41 for $u = 1$ (upper

curves) and 1.81 for $u = -0.5$ (lower curves), respectively, compared to 2 for the linearized model ($u \to 0$) in the SPIM ($G = 0$). The respective values are 6.46 and 5.74 versus 6 for $G = 2$. While the difference is similar on an absolute scale here, it becomes considerably smaller relative to the velocity itself. So the effect of the nonlinearity decreases with increasing G, that is, toward the transport-limited model.

Since sharpening and stretching of knickpoints is also related to the effect of nonlinearity on the velocity of migration, basically the behavior is observed for the shape of the knickpoints. Comparing the upper and lower curves in Figure 11 for the SPIM reveals that the knickpoints do not only migrate at different velocities, but also that the knickpoints in the lower curves are clearly stretched at long times, while those in the upper curves remain sharp except for some numerical diffusion. In turn, the shapes of the upper and lower profiles are quite similar for $G = 1$ and also similar to the linear version (Figure 4b). So sharpening and stretching of knickpoints is already quite small for $G = 1$ if the uplift rate varies by a factor of two compared to the initial equilibrium ($u = 1$ and $u = -0.5$ at $U_0 = 1$). This effect becomes stronger for $G = 2$. So there are still differences in the velocity of migration between the upper and lower curves, but sharpening and stretching of knickpoints appears to be negligible here.

11. Vertical Rates of Knickpoint Migration

While the theory based on the χ transform is well-suited for advanced analyses, investigating how knickpoints migrate vertically is more intuitive. As already discussed in Section 5, the SPIM predicts a constant vertical rate of knickpoint migration for $n = 1$ under specific conditions. This fundamental property is generalized with regard to the nonlinear model and to sediment transport in the following.

Let us follow the knickpoint upstream or, to be more precise, a point slightly above the knickpoint, given by a function $\chi(t)$ and track its elevation $H(\chi(t), t)$. This point is uplifted at a rate u, while its channel slope is still the same as for the initial topography H_0. Thus, its vertical rate of migration is

$$\frac{dH}{dt} = \frac{\partial H}{\partial \chi}\frac{d\chi}{dt} + \frac{\partial H}{\partial t} = \frac{\partial H_0}{\partial \chi}\frac{d\chi}{dt} + u. \tag{47}$$

Using Equation 46 that describes the horizontal velocity of knickpoint migration and the equilibrium condition (Equation 41), this relation can be simplified to

$$\frac{dH}{dt} = nK_\mathrm{d}\left(\frac{\partial H_0}{\partial \chi}\right)^n F(\gamma) + u = U_0\frac{K_\mathrm{d}}{K}nF(\gamma) + u. \tag{48}$$

For the linear version of the SPIM ($K = K_\mathrm{d}$, $n = 1$, $F(\gamma) = 1$), this relation collapses to

$$\frac{dH}{dt} = U_0 + u = U, \tag{49}$$

which reproduces the result that knickpoints follow the uplifted rock (Whipple & Tucker, 1999). If the order of magnitude of the uplift rate is known, this relation provides an idea of how long a knickpoint initiated at a given location could migrate upstream until it is lost at the drainage divide or at the hillslopes. Similarly, it can be used for estimating at which time an existing knickpoint was initiated if the location of the fault is known or vice versa.

For the general situation, Equation 48 typically predicts a faster vertical migration. So knickpoints are typically running ahead of the uplifted rock. Both sediment transport and nonlinearity contribute to this phenomenon. The effect of sediment transport is represented by the factor $\frac{K_\mathrm{d}}{K} = 1 + G$ in Equation 48. As already discussed in Section 10, the effect of nonlinearity consists of two components, where an increase in rate typically occurs for $n > 1$. Primarily, there is a factor of n that describes the increase for small changes u in uplift rate, while the component $F(\gamma)$ (Equations 39 and 45) is a correction for larger u.

12. Implications

As found in the previous sections, sediment transport does not affect the properties of knickpoints qualitatively. As an immediate implication for landform evolution modeling, we cannot conclude from the existence of distinct knickpoints alone that sediment transport is unimportant for fluvial landform evolution in the respective region.

So neglecting sediment transport in fluvial landform evolution, for example, by using the SPIM, cannot be justified by the existence of knickpoints alone.

The implications of the results on the role of rivers as tectonic (or climatic) archives are more complex. While rivers still record the history unless they are fully transport-limited, sensitivity and capacity of the recorder are reduced by sediment transport.

First, the same tectonic signal causes a weaker change in channel steepness and thus a smaller difference in channel steepness across the knickpoint compared to the SPIM. In addition, this difference decreases further while mobile knickpoints migrate upstream, which was described as knickpoint flattening in Section 6. If we assume that only knickpoints with a given minimum difference in channel steepness can be detected reliably, sediment transport reduces the sensitivity of the knickpoint archive to tectonic signals.

Second, mobile knickpoints migrate upstream faster than in the SPIM at the same effective erodibility K, which has an immediate effect on the time span covered by the archive. As an example, the theory of Whipple and Tucker (1999) for the linear version of the SPIM predicts that an available upstream difference in elevation of 1,000 m along the river from a fault would theoretically allow for an archive covering 4 million years at an uplift rate of 0.25 mm per year. According to the results of Section 11, sediment transport reduces this time span by a factor $\frac{K_\mathrm{d}}{K} = 1 + G$. Based on the preliminary estimate $G = 1.6n^{-1.1}$ proposed by Guerit et al. (2019, data supplement), the increase in velocity compared to the linear version would be a factor of $(1 + G)n \approx 2.5$ for $1 \leq n \leq 3$ if the change in uplift u is small. In this case, the tectonic archive would only cover about 1.5 million years instead of 4 million years.

Third, the response of the sediment flux to a tectonic signal is faster in small catchments as shown in Section 7. As a consequence, the second phase of adjustment (after the mobile knickpoint has passed) is also faster in small catchments. In principle, this result also holds for tributaries. This leads to a temporary loss of the collinearity of the trunk stream and its tributaries in a χ-plot, which is a fundamental property of the SPIM. Owing to their faster response, tributaries will temporarily be steeper than the trunk stream in a χ-plot in response to an increase in uplift rate. So some caution is required when using the collinearity of tributaries for estimating the concavity index θ (e.g., Hergarten et al., 2016).

13. Conclusions

The most important result of this study is that sediment transport does not cause a smearing of mobile knickpoints at least for the simplest extension of the SPIM by sediment transport. This may be surprising since the shared stream-power model used in this study covers the entire range from pure bedrock incision to the transport-limited model, which does not support sharp mobile knickpoints at all.

In terms of the shared stream-power model, the detachment-limited erodibility K_d dictates the initial response to tectonic signals, which suggests that sediment transport has no effect on the initial response. However, when comparing rivers with the same steepness at the same overall erosion rate (so at the same effective erodibility), K_d increases with increasing relevance of sediment transport. Then the velocity of knickpoint migration increases when moving from the SPIM toward the transport-limited model. This leads to a shorter lifetime of knickpoints until they arrive at the drainage divide. So knickpoints leave the domain rapidly instead of being smeared if we approach the transport-limited model. However, some flattening occurs in the sense that the difference in channel steepness across the knickpoint decreases while the knickpoint migrates upstream.

Nonlinearity has qualitatively the same effect on the migration of mobile knickpoints as in the SPIM. Knickpoints arising from small changes in uplift migrate by a factor n (the slope exponent in the stream-power law) faster than in the linear model. So sediment transport may have the same effect on knickpoint velocity as an exponent $n > 1$ in the SPIM. As a major difference toward the SPIM, however, tributaries are not necessarily collinear to the trunk stream in a χ-plot if sediment transport is included in the model.

Convex knickpoints move faster than concave knickpoints for $n > 1$ and vice versa. Concave knickpoints are lost through time by stretching for $n > 1$, while this happens to convex knickpoints for $n < 1$. As the main difference toward the SPIM, however, sediment transport considerably reduces the effect of nonlinearity on the properties of mobile knickpoints.

In contrast to the SPIM, stationary tectonic knickpoints are not immediately steady in the shared stream-power model. The overall channel steepness around a concave knickpoint slowly increases through time due to the increasing sediment flux from the upstream region and vice versa. In the linear model, the difference in channel steepness across the knickpoint remains constant, while nonlinearity results in a flattening of concave steady knickpoints (increasing uplift) for $n > 1$ through time and vice versa.

Conflict of Interest

The author declares no conflicts of interest relevant to this study.

Data Availability Statement

Codes and results of the simulations are available at the FreiDok data repository 219668 (Hergarten, 2021a). The open-source landform evolution model OpenLEM is freely available at http://hergarten.at/openlem. Interested users are advised to download the most recent version of OpenLEM. The author is happy to assist interested readers in reproducing the results and performing subsequent research.

Acknowledgments
The thorough and constructive reviews by K. Whipple and two anonymous reviewers, which strongly improved the accessibility of the study, are greatly appreciated. Furthermore, the author would like to thank the editors Adam M. Booth and M. Attal for their support. Open access funding enabled and organized by Projekt DEAL.

References

Adams, B. A., Whipple, K. X., Forte, A. M., Heimsath, M., & Hodges, K. V. (2020). Climate controls on erosion in tectonically active landscapes. *Science Advances*, *6*(42), eaaz3166. https://doi.org/10.1126/sciadv.aaz3166

Beckers, A., Bovy, B., Hallot, E., & Demoulin, A. (2015). Controls on knickpoint migration in a drainage network of the moderately uplifted Ardennes Plateau, Western Europe. *Earth Surface Processes and Landforms*, *40*, 357–374. https://doi.org/10.1002/esp.3638

Campforts, B., & Govers, G. (2015). Keeping the edge: A numerical method that avoids knickpoint smearing when solving the stream power law. *Journal of Geophysical Research: Earth Surface*, *120*, 1189–1205. https://doi.org/10.1002/2014jf003376

Campforts, B., Schwanghart, W., & Govers, G. (2017). Accurate simulation of transient landscape evolution by eliminating numerical diffusion: The TTLEM 1.0 model. *Earth Surface Dynamics*, *5*, 47–66. https://doi.org/10.5194/esurf-5-47-2017

Castelltort, S., Goren, L., Willett, S. D., Champagnac, J.-D., Herman, F., & Braun, J. (2012). River drainage patterns in the New Zealand alps primarily controlled by plate tectonic strain. *Nature Geoscience*, *5*, 744–748. https://doi.org/10.1038/ngeo1582

Davis, W. M. (1899). The geographical cycle. *Geographical Journal*, *14*(5), 481–504. https://doi.org/10.2307/1774538

Davy, P., & Lague, D. (2009). Fluvial erosion/transport equation of landscape evolution models revisited. *Journal of Geophysical Research: Earth Surface*, *114*, F03007. https://doi.org/10.1029/2008JF001146

Gailleton, B., Mudd, S. M., Clubb, F. J., Peifer, D., & Hurst, M. (2019). A segmentation approach for the reproducible extraction and quantification of knickpoints from river long profiles. *Earth Surface Dynamics*, *7*, 211–230. https://doi.org/10.5194/esurf-7-211-2019

Gasparini, N. M., Bras, R. L., & Whipple, K. X. (2006). Numerical modeling of non–steady-state river profile evolution using a sediment-flux-dependent incision model. In S. D. Willett, N. Hovius, M. T. Brandon, & D. M. Fisher (Eds.), *Tectonics, climate, and landscape evolution* (Vol. 398, pp. 127–141). Geological Society of America. https://doi.org/10.1130/2006.2398(08)

Gasparini, N. M., Whipple, K. X., & Bras, R. L. (2007). Predictions of steady state and transient landscape morphology using sediment-flux-dependent river incision models. *Journal of Geophysical Research: Earth Surface*, *112*, F03S09. https://doi.org/10.1029/2006JF000567

Gilbert, G. K. (1877). *Report on the geology of the Henry Mountains (Tech. Rep.)*. US Geol. Survey. https://doi.org/10.3133/70039916

Guerit, L., Yuan, X. P., Carretier, S., Bonnet, S., Rohais, S., Braun, J., & Rouby, D. (2019). Fluvial landscape evolution controlled by the sediment deposition coefficient: Estimation from experimental and natural landscapes. *Geology*, *47*(9), 853–856. https://doi.org/10.1130/G46356.1

Hack, J. T. (1957). *Studies of longitudinal profiles in Virginia and Maryland (No. 294-B)*. US Government Printing Office. https://doi.org/10.3133/pp294B

Harel, M.-A., Mudd, S. M., & Attal, M. (2016). Global analysis of the stream power law parameters based on worldwide ^{10}Be denudation rates. *Geomorphology*, *268*, 184–196. https://doi.org/10.1016/j.geomorph.2016.05.035

Haviv, I., Enzel, Y., Whipple, K. X., Zilberman, E., Matmon, A., Stone, J., & Fifield, K. L. (2010). Evolution of vertical knickpoints (waterfalls) with resistant caprock: Insights from numerical modeling. *Journal of Geophysical Research: Earth Surface*, *115*, F03028. https://doi.org/10.1029/2008JF001187

Hergarten, S. (2020a). Rivers as linear elements in landform evolution models. *Earth Surface Dynamics*, *8*, 367–377. https://doi.org/10.5194/esurf-8-367-2020

Hergarten, S. (2020b). Transport-limited fluvial erosion – Simple formulation and efficient numerical treatment. *Earth Surface Dynamics*, *8*, 841–854. https://doi.org/10.5194/esurf-8-841-2020

Hergarten, S. (2021a). *The influence of sediment transport on stationary and mobile knickpoints in river profiles: Codes and data*. Albert-Ludwigs-Universität Freiburg. https://doi.org/10.6094/UNIFR/219668

Hergarten, S. (2021b). Modeling glacial and fluvial landform evolution at large scales using a stream-power approach. *Earth Surface Dynamics*, *9*, 937–952. https://doi.org/10.5194/esurf-9-937-2021

Hergarten, S., & Neugebauer, H. J. (2001). Self-organized critical drainage networks. *Physical Review Letters*, *86*, 2689–2692. https://doi.org/10.1103/PhysRevLett.86.2689

Hergarten, S., Robl, J., & Stüwe, K. (2016). Tectonic geomorphology at small catchment sizes—Extensions of the stream-power approach and the χ method. *Earth Surface Dynamics*, *4*, 1–9. https://doi.org/10.5194/esurf-4-1-2016

Hilley, G. E., Porder, S., Aron, F., Baden, C. W., Johnstone, S. A., Liu, F., et al. (2019). Earth's topographic relief potentially limited by an upper bound on channel steepness. *Nature Geoscience*, *12*, 828–832. https://doi.org/10.1038/s41561-019-0442-3

Howard, A. D. (1994). A detachment-limited model for drainage basin evolution. *Water Resources Research*, *30*, 2261–2285. https://doi.org/10.1029/94WR00757

Kooi, H., & Beaumont, C. (1994). Escarpment evolution on high-elevation rifted margins: Insights derived from a surface process model that combines diffusion, advection and reaction. *Journal of Geophysical Research*, *99*, 12191–12209. https://doi.org/10.1029/94jb00047

Kwang, J. S., & Parker, G. (2017). Landscape evolution models using the stream power incision model show unrealistic behavior when m/n equals 0.5. *Earth Surface Dynamics*, *5*, 807–820. https://doi.org/10.5194/esurf-5-807-2017

Lague, D. (2014). The stream power river incision model: Evidence, theory and beyond. *Earth Surface Processes and Landforms*, *39*, 38–61. https://doi.org/10.1002/esp.3462

Lyons, N. J., Val, P., Albert, J. S., Willenbring, J. K., & Gasparini, N. M. (2020). Topographic controls on divide migration, stream capture, and diversification in riverine life. *Earth Surface Dynamics*, *8*, 893–912. https://doi.org/10.5194/esurf-8-893-2020

Neely, A. B., Bookhagen, B., & Burbank, D. W. (2017). An automated knickzone selection algorithm (KZ-Picker) to analyze transient landscapes: Calibration and validation. *Journal of Geophysical Research: Earth Surface*, *122*, 1236–1261. https://doi.org/10.1002/2017JF004250

Pelletier, J. D. (2010). Minimizing the grid-resolution dependence of flow-routing algorithms for geomorphic applications. *Geomorphology*, *122*, 91–98. https://doi.org/10.1016/j.geomorph.2010.06.001

Perron, J. T., Dietrich, W. E., & Kirchner, J. W. (2008). Controls on the spacing of first-order valleys. *Journal of Geophysical Research: Earth Surface*, *113*, F04016. https://doi.org/10.1029/2007JF000977

Perron, J. T., & Royden, L. (2013). An integral approach to bedrock river profile analysis. *Earth Surface Processes and Landforms*, *38*, 570–576. https://doi.org/10.1002/esp.3302

Queiroz, G. L., Salamuni, E., & Nascimento, E. R. (2015). Knickpoint finder: A software tool that improves neotectonic analysis. *Computers & Geosciences*, *76*, 80–87. https://doi.org/10.1016/j.cageo.2014.11.004

Robl, J., Hergarten, S., & Prasicek, G. (2017). The topographic state of fluvially conditioned mountain ranges. *Earth-Science Reviews*, *168*, 290–217. https://doi.org/10.1016/j.earscirev.2017.03.007

Royden, L., & Perron, J. T. (2013). Solutions of the stream power equation and application to the evolution of river longitudinal profiles. *Journal of Geophysical Research: Earth Surface*, *118*(2), 497–518. https://doi.org/10.1002/jgrf.20031

Schwanghart, W., & Scherler, D. (2014). Short communication: TopoToolbox 2—MATLAB-based software for topographic analysis and modeling in Earth surface sciences. *Earth Surface Dynamics*, *2*, 1–7. https://doi.org/10.5194/esurf-2-1-2014

Shobe, C. M., Tucker, G. E., & Barnhart, K. R. (2017). The SPACE 1.0 model: A Landlab component for 2-D calculation of sediment transport, bedrock erosion, and landscape evolution. *Geoscientific Model Development*, *10*, 4577–4604. https://doi.org/10.5194/gmd-10-4577-2017

Sklar, L., & Dietrich, W. E. (1998). River longitudinal profiles and bedrock incision models: Stream power and the influence of sediment supply. In K. J. Tinkler, & E. Wohl (Eds.), *Rivers over rock: Fluvial processes in bedrock channels* (pp. 237–260). American Geophysical Union. https://doi.org/10.1029/GM107p0237

Turowski, J. M. (2012). Semi-alluvial channels and sediment-flux-driven bedrock erosion. In M. Church, P. Biron, & A. Roy (Eds.), *Gravel-bed rivers* (pp. 399–418). John Wiley & Sons, Ltd. https://doi.org/10.1002/9781119952497.ch29

Whipple, K. X., DiBiase, R. A., & Crosby, B. T. (2013). Bedrock rivers. In J. Shroder, & E. Wohl (Eds.), *Fluvial geomorphology* (Vol. 9, pp. 550–573). Academic Press. https://doi.org/10.1016/b978-0-12-374739-6.00254-2

Whipple, K. X., & Tucker, G. E. (1999). Dynamics of the stream power river incision model: Implications for height limits of mountain ranges, landscape response time scales and research needs. *Journal of Geophysical Research*, *104*, 17661–17674. https://doi.org/10.1029/1999JB900120

Whipple, K. X., & Tucker, G. E. (2002). Implications of sediment-flux-dependent river incision models for landscape evolution. *Journal of Geophysical Research*, *107*(B2), 2039. https://doi.org/10.1029/2000JB000044

Willett, S. D., McCoy, S. W., Perron, J. T., Goren, L., & Chen, C.-Y. (2014). Dynamic reorganization of river basins. *Science*, *343*, 1248765. https://doi.org/10.1126/science.1248765

Willgoose, G. (2005). Mathematical modeling of whole landscape evolution. *Annual Review of Earth and Planetary Sciences*, *33*, 443–459. https://doi.org/10.1146/annurev.earth.33.092203.122610

Wobus, C., Whipple, K. X., Kirby, E., Snyder, N., Johnson, J., Spyropolou, K., & Sheehan, D. (2006). Tectonics from topography: Procedures, promise, and pitfalls. In S. D. Willett, N. Hovius, M. T. Brandon, & D. M. Fisher (Eds.), *Tectonics, climate, and landscape evolution* (Vol. 398, pp. 55–74). Geological Society of America. https://doi.org/10.1130/2006.2398(04)

Yuan, X. P., Braun, J., Guerit, L., Rouby, D., & Cordonnier, G. (2019). A new efficient method to solve the stream power law model taking into account sediment deposition. *Journal of Geophysical Research: Earth Surface*, *124*(6), 1346–1365. https://doi.org/10.1029/2018JF004867